Solidification Thermal Parameters Affecting the Columnar-to-Equiaxed Transition

CLÁUDIO A. SIQUEIRA, NOÉ CHEUNG, and AMAURI GARCIA

Experiments were conducted to analyze the columnar-to-equiaxed transition (CET) during the upward unsteady-state directional solidification of Al-Cu and Sn-Pb alloys, under different conditions of superheat and heat-transfer efficiencies at the metal/mold interface. A combined theoretical and experimental approach is developed to quantitatively determine the solidification thermal parameters: transient heat-transfer coefficients, tip growth rates, thermal gradients, and cooling rates. The observed results do not give support to CET criteria based individually either on tip growth rate or temperature gradients ahead of the liquidus isotherm. Rather, the analysis has indicated that a more convenient criterion should encompass both thermal parameters through the tip cooling rate. The columnar growth is expected to prevail throughout the casting for a tip cooling rate higher than a critical value, which depends only on the alloy system and was observed to be about 0.2 K/s for Al-Cu alloys and 0.01 K/s for Sn-Pb alloys in the present investigation.

I. INTRODUCTION

THE macrostructure of cast ingots generally consists of three distinct zones. These are the chill, columnar, and equiaxed zones respectively. The origin of each one has been the subject of intense experimental and theoretical investigation because of the well-known correlation between grain structures and mechanical properties. All three zones may or may not be present in a particular case. However, when a casting contains columnar and equiaxed grains, the columnar-to-equiaxed transition (CET) is usually narrow.[1] Lack of a quantitative understanding of the relationship between casting thermal conditions and the resulting structure has limited the development of certain procedures and methods for quality castings.

In previous work, the CET was proposed to be caused either by a pileup of equiaxed crystals that blocked the growth of the columnar grains or by attachment of equiaxed crystals from the liquid to the columnar dendrite front.[2] The CET was found to depend on casting parameters such as alloy system and composition, casting size, mold material, mold temperature, pouring superheat, heat-transfer coefficients at the metal/mold interface, melt convection, and the presence of nucleating agents.[3–7] Only recently has the CET been the subject of theoretical studies undertaken with a view toward modeling this phenomenon, as reviewed by Flood and Hunt.[1] These studies, as well as the latest models, highlight the importance of the relative growth of the equiaxed and columnar grains and develop expressions or numerical procedures to describe the criterion for the columnar-to-equiaxed transition, generally in terms of tip growth rate and temperature gradients ahead of the dendrite tips.[7–12]

Hunt and co-workers[13–16] have developed a model for the CET based on metal supercooling, which qualitatively reveals the influences of alloy composition, density of nucleating sites, temperature gradient in the melt (G_L), and tip growth rate (v_L). Wang and Beckermann[3] developed a numerical model to calculate the CET position based on a multiphase approach, which accounts for heat and solute diffusion, as well as for grain nucleation, growth, and morphology.

A number of experimental investigations reported in the literature suggest that the CET occurs when the temperature gradient in the melt reachs a minimum critical value. Weinberg and co-workers found values of 0.10 °C/mm and 0.13 °C/mm, respectively, for Sn 5 wt pct Pb and Sn 15 wt pct Pb alloys[9] and of 0.06 °C/mm for an Al 3 wt pct Cu alloy.[10] Suri *et al.*,[7] analyzing the directional solidification of an Al 4.5 wt pct Cu alloy in copper and stainless steel chills and under a broad range of superheats, after comparing CET positions with the corresponding values of G_L and v_L, have suggested that the transition occurs for $G_L < 0.74\ v_L^{0.64}$. More recently, Ares and Schvezov[11] have performed experiments with lead-tin alloys directionally solidified from a chill face and observed that the CET occurs in a zone rather than in a sharp plane when the temperature gradient in the melt decreased to values ranging from −0.8 °C/cm to 1 °C/cm. Gandin,[12] combining simulations furnished by a numerical solidification model and experimental results concerning the directional solidification of Al-Si alloys, proposed a CET criterion based on the position of the maximum velocity of the columnar/dendritic interface, suggesting a continuous increase in tip growth rate up to a maximum value about two-thirds the length of the ingot, where the transition is supposed to occur.

In the present article, an investigation was undertaken to examine experimentally the CET in Al-Cu and Sn-Pb alloys directionally solidified in a cooled mold, under different conditions of superheat and heat-transfer efficiencies at the metal/mold interface. A combined theoretical and experimental approach is developed to quantitatively determine the solidification thermal parameters, *i.e.*, transient heat-transfer coefficients, tip growth rates, thermal gradients, and cooling rate, which affect the structure transition.

CLÁUDIO A. SIQUEIRA and NOÉ CHEUNG, Doctoral Students and Research Assistants, and AMAURI GARCIA, Professor, are with the Department of Materials Engineering, State University of Campinas—Unicamp, 13083-970 Campinas SP, Brazil. Contact e-mail: amaurig@fem.unicamp.br

Manuscript submitted July 9, 2001.

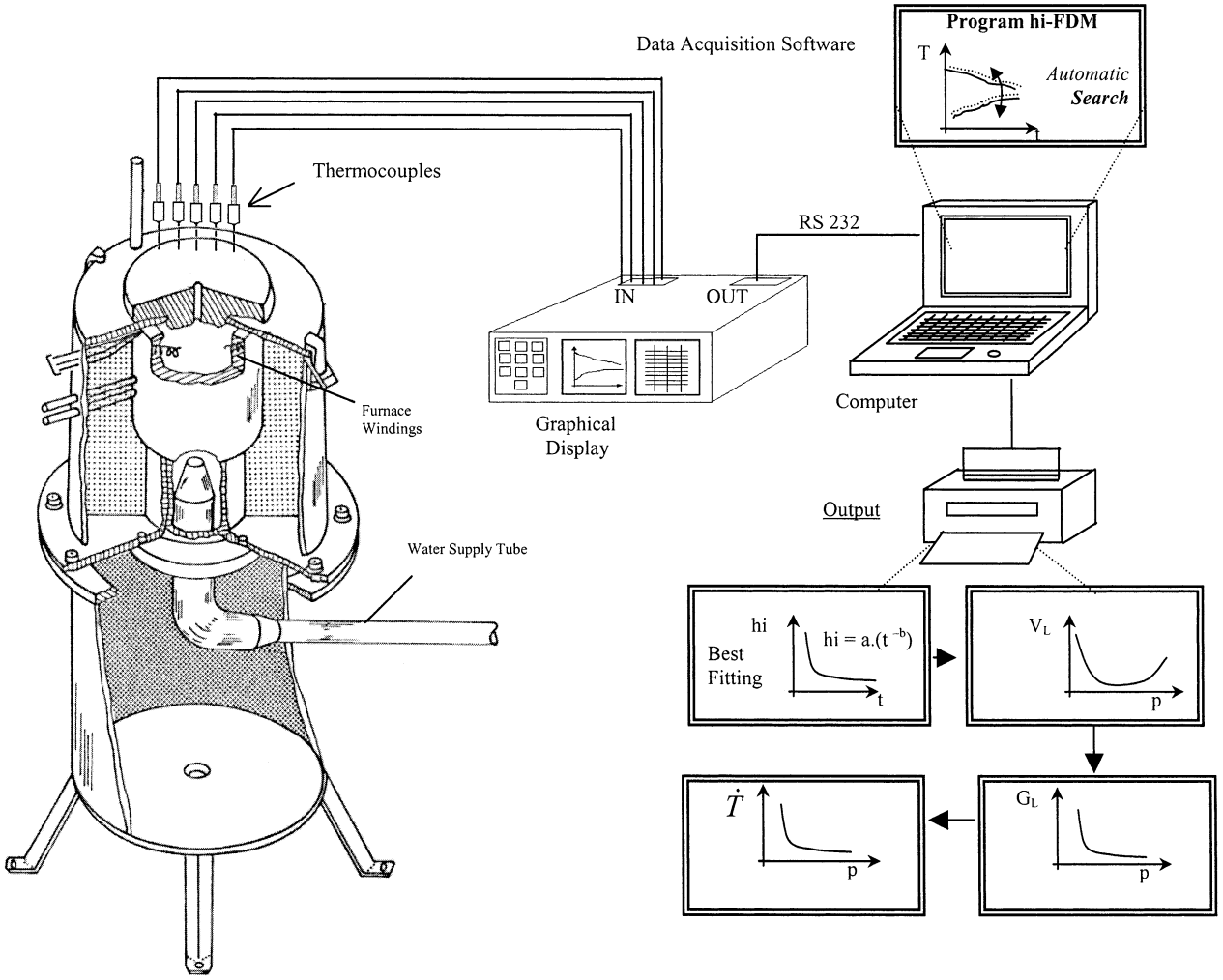

Fig. 1—Schematic representation of the experimental setup.

II. EXPERIMENTAL PROCEDURE

The casting assembly used in solidification experiments is shown in Figure 1. The solidification apparatus was designed in such a way that the heat was extracted only through the water-cooled bottom, promoting upward directional solidification. The use of such experimental configuration permits natural convection to be minimized, as well as solute convection due to buoyancy forces, if the rejected solute has a higher density than the alloy melt. A stainless steel mold was used, which had an internal diameter of 50 mm, height 110 mm, and wall thickness 5 mm. The inner vertical surface was covered with a layer of insulating alumina to minimize radial heat losses, and a top cover made of an insulating material was used to reduce heat losses from the metal/air surface. The bottom part of the mold was closed with a thin (3 mm) disc of carbon steel. The alloys were melted *in situ* and the lateral electric heaters had their power controlled in order to permit a desired superheat to be achieved. To begin solidification, the electric heaters were disconnected, and at the same time, the water flow was initiated.

Experiments were carried out with Al-Cu alloys (2.0, 5.0, 8.0, and 10 wt pct Cu) and Sn-Pb alloys (10 and 30 wt pct Pb) at various superheats. The chemical compositions of metals that were used to prepare these alloys are presented in Table I. The employed thermophysical properties are derived from those reported in a previous article.[19] Some experiments were performed under two sets of thermal contact conditions at the metal/mold interface, corresponding to the heat extracting surface being polished or coated with an alumina-based mold wash. In the coated case, the mold wash was applied over the internal surface of the steel sheet with a spray gun, and the coating film thickness was standardized at about 100 μm.

Temperatures in the casting were monitored during solidification *via* the output of a bank of type K thermocouples (1.6-mm diameter) accurately positioned with respect to the heat extracting surface. The thermocouples were calibrated at the melting points of aluminum (for Al-Cu alloys) and tin (for Sn-Pb alloys), exhibiting fluctuations of about 1.0 °C and 0.4 °C, respectively. All of the thermocouples were connected by coaxial cables to a data logger interfaced with a computer, and the temperature data were acquired automatically.

The cylindrical ingots were sectioned on a midplane, mechanically polished using abrasive papers, and etched with an acid solution (15 ml HF; 4.5 ml HNO_3; 9 ml HCl and 271.5 ml H_2O, for Al-Cu alloys and 100 ml H_2O;

Table I. Chemical Analyses of Metals Used to Prepare Al-Cu and Sn-Pb Alloys

	Chemical Compositions (Wt Pct)									
Metal	Fe	Ni	Cu	Si	Mg	Pb	Cr	Mn	Zn	Sn
Al	0.182	0.0148	0.0242	0.103	0.0013	—	—	—	—	—
Cu	—	—	—	0.09	—	0.002	0.27	—	—	—
Sn	0.009	—	0.007	—	—	0.19	—	0.0025	—	—
Pb	0.002	0.003	—	—	—	—	—	—	0.003	0.25

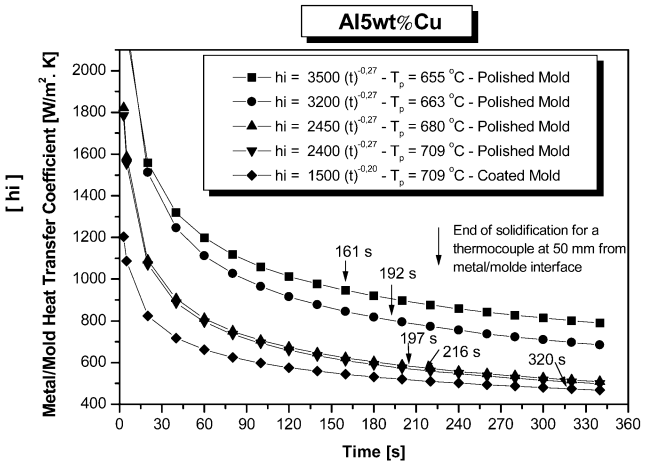

Fig. 2—Evolution of the metal/mold heat-transfer coefficients as a function of superheat: Al 5 wt pct Cu.

2 ml HCl and 10 g $FeCL_3$, for Sn-Pb alloys) to reveal the macrostructure. The CET, if any, was measured from the bottom of the casting. Selected sections on both sides of the transition were electropolished and etched with a solution (10 pct NaOH in distillated water, for Al-Cu alloys) for micrograph examination. An image processing system Neophot 32 (Carl Zeiss, Esslingen, Germany) and Leica Q-500 MC (Leica Imaging Systems Ltd, Cambridge, England) were then used to measure dendrite spacings (20 measurements for each selected position).

III. RESULTS AND DISCUSSION

The temperature files containing the experimentally monitored temperatures were used in a finite difference heat flow program[17,18] to determine the transient metal/mold heat-transfer coefficient, h_i, as described in a previous article.[19] Figure 2 shows a typical example of the time dependence of the metal/mold heat-transfer coefficients (h_i) during the course of different experiments of upward directional solidification of a Al 5 wt pct Cu alloy. Table II summarizes all the values of h_i, expressed as a power function of time, determined during the present experimental investigation for Al-Cu and Sn-Pb alloys under different conditions of melt superheat. While heat-transfer coefficients are operative at both coolant/mold and mold/casting interfaces, here, h_i represents a global value describing coolant/casting heat exchange.

It can be seen both in Table II and Figure 2 that, as expected, under the same condition of melt superheat, the heat-transfer coefficient decreases when the mold surface is coated with an insulating layer of alumina. It can also be observed that the increase in melt superheat decreases the heat-transfer coefficient. This is, apparently, in contradiction with results obtained in a previous article concerning the horizontal directional solidification of Al-Cu and Sn-Pb alloys[19] and can be explained by the differences in the physical configuration of the two experimental setups. Figure 3 shows typical results of the time dependence of the metal mold heat-transfer coefficients obtained during the course of solidification of a Sn 10 pct Pb alloy, in both vertical and horizontal directional solidification experiments. It can be seen that, for horizontal solidification experiments, higher h_i profiles are obtained as the melt superheat is increased. A reverse situation can be observed during vertical solidification with h_i decreasing as the melt superheat is increased. In both cases, the superheat delays the solidification evolution. In the horizontal solidification, this will translate to a higher h_i profile for higher melt superheats, because the contraction of metal from the mold wall will also be delayed. In the upward solidification, the casting weight will contribute to a better metal/mold thermal contact if lateral contraction is effective (permitting the ingot to be gradually detached from lateral walls). This will happen sooner for solidification without superheat, and as a consequence, a higher h_i profile will be provided with decreasing melt superheat.

The results of thermal analysis have also been used to determine the displacement of the liquidus isotherm. In order to determine the solidification thermal parameters such as the tip growth rate, v_L, thermal gradient in the liquid at the right of the tip interface, G_L, and the cooling rate, $\dot{T}$, a numerical model was developed to simulate the solidification of binary alloys in a cylindrical cavity chilled from below. Initially, the alloys were assumed to be molten, quiescent, and uniformly mixed, with temperatures exceeding the liquidus temperatures. The top and side walls were assumed to be insulated, while energy was extracted from the bottom at a rate governed by the metal/mold heat-transfer coefficient. The mathematical formulation of this solidification problem is given by the one-dimensional heat conduction equation:[20]

$$\rho \cdot c \cdot \frac{\partial T}{\partial t} = \frac{\partial}{\partial x}\left(K(x)\,\frac{\partial T}{\partial x}\right) + \dot{q} \qquad [1]$$

where

K = thermal conductivity (W/m K),
c = specific heat (J/kg K),
ρ = density (kg/m^3),
$\dot{q}$ = rate of energy generation (W/m^3),
T = temperature (K),
t = time (s), and
x = rectangular coordinate (m).

Table II. Metal/Mold Heat-Transfer Coefficients during the Upward Directional Solidification in a Water Cooled Mold

Alloy	Pouring Temperature T_p (K) and Mold Surface Condition	h_i (W/m^2 K), t (s)
Al 2 wt pct Cu	T_p = 660 °C—polished mold	$h_i = 2600\ (t)^{-0.14}$
	T_p = 674 °C—polished mold	$h_i = 2100\ (t)^{-0.14}$
	T_p = 689 °C—polished mold	$h_i = 2000\ (t)^{-0.14}$
	T_p = 709 °C—polished mold	$h_i = 1850\ (t)^{-0.14}$
	T_p = 689 °C—coated mold	$h_i = 1900\ (t)^{-0.18}$
Al 5 wt pct Cu	T_p = 655 °C—polished mold	$h_i = 3500\ (t)^{-0.27}$
	T_p = 663 °C—polished mold	$h_i = 3200\ (t)^{-0.27}$
	T_p = 680 °C—polished mold	$h_i = 2450\ (t)^{-0.27}$
	T_p = 709 °C—polished mold	$h_i = 2400\ (t)^{-0.27}$
	T_p = 709 °C—coated mold	$h_i = 1500\ (t)^{-0.20}$
Al 8 wt pct Cu	T_p = 640 °C—polished mold	$h_i = 5100\ (t)^{-0.33}$
	T_p = 652 °C—polished mold	$h_i = 5100\ (t)^{-0.33}$
	T_p = 690 °C—polished mold	$h_i = 5100\ (t)^{-0.33}$
	T_p = 652 °C—coated mold	$h_i = 1000\ (t)^{-0.065}$
Al 10 wt pct Cu	T_p = 700 °C—polished mold	$h_i = 5700\ (t)^{-0.33}$
	T_p = 705 °C—coated mold	$h_i = 1000\ (t)^{-0.075}$
Sn 10 wt pct Pb	T_p = 220 °C—coated mold	$h_i = 950\ (t)^{-0.01}$
Sn 30 wt pct Pb	T_p = 197 °C—coated mold	$h_i = 1100\ (t)^{-0.01}$

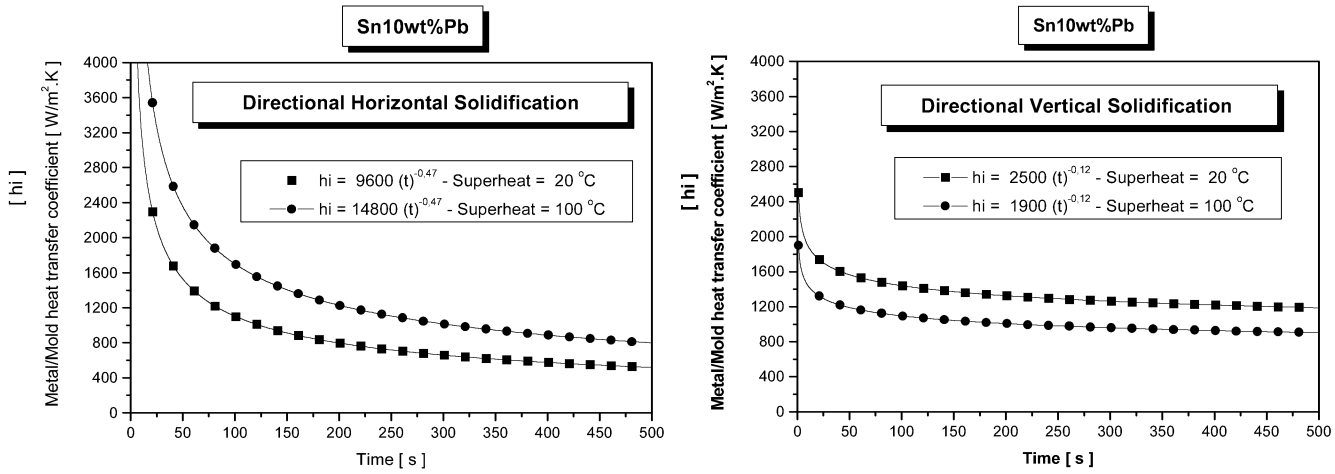

Fig. 3—Time dependence of the metal/mold heat transfer coefficient during vertical and horizontal directional solidification of a Sn 10 wt pct Pb all oy.

The release of latent heat between the liquidus and solidus temperatures is expressed by $\dot{q}$:

$$\dot{q} = \rho \cdot L \cdot \frac{\partial f_s}{\partial t} \qquad [2]$$

where

L = latent heat (J/kg), and
f_s = local solid fraction (pct).

The fraction of solid in the mushy zone is estimated by the Scheil equation, which assumes perfect mixing in the liquid and no solid diffusion. With the liquidus and solidus having constant slopes, f_s is then expressed as

$$f_s = 1 - \left(\frac{T_f - T}{T_f - T_{\text{Liq}}}\right)^{\frac{1}{k-1}} \qquad [3]$$

where

T_f = melting temperature (K),
T_{Liq} = liquidus temperature (K), and
k = partition coefficient.

The latent heat released during solidification of the remaining liquid of eutectic composition was taken into account by a device, which considers a temperature accumulation factor.

Substituting Eq. [2] into Eq. [1] gives

$$\rho \cdot c' \cdot \frac{\partial T}{\partial t} = \frac{\partial}{\partial x}\left(K(x)\,\frac{\partial T}{\partial x}\right) \qquad [4]$$

where c' can be considered as a pseudo-specific heat:[21]

$$c' = c_M - L \cdot \frac{\partial f_s}{\partial T} \qquad [5]$$

$$c_M = (1 - f_s) \cdot c_L + f_s \cdot c_s \qquad [6]$$

where the subscripts S, L, and M refer to solid, liquid, and mushy, respectively.

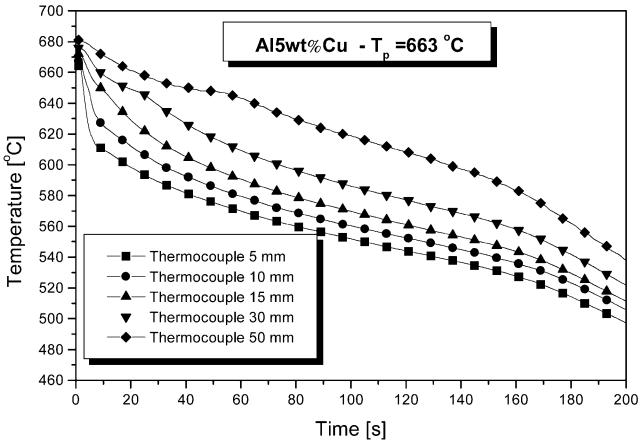

(*a*)

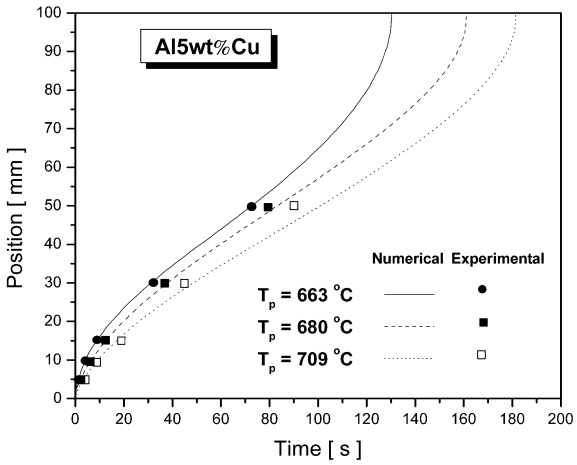

(*b*)

Fig. 4—Typical experimental thermal response of temperature *vs* time for five thermocouples located at different positions from metal/mold interface (*a*) and (*b*) position of the liquidus isotherm as a function of time: Al 5 wt pct Cu, polished mold and different degrees of melt superheat.

A finite difference form of Eq. [4] is obtained for the time-dependent temperature distribution at discrete grid points:

$$T_i^{n+1} = \frac{\Delta t}{(\rho \cdot c')_i \cdot \Delta x^2} [K_{eq_{i+1}} \cdot (T_{i+1}^n - T_i^n) + K_{eq_{i-1}} \cdot (T_{i-1}^n - T_i^n)] + T_i^n \quad [7]$$

where n and $n + 1$ refer to temperatures before and after the incremental time interval Δt, i is the element position according to x-axes, and K_{eq} is the equivalent thermal conductivity in terms of the thermal conductivity of an adjacent element and itself, given by

$$K_{eq_{i+1}} = \frac{2K_{i+1} \cdot K_i}{K_{i+1} + K_i} \quad [8]$$

$$K_{eq_{i-1}} = \frac{2K_{i-1} \cdot K_i}{K_{i-1} + K_i} \quad [9]$$

A two-dimensional version of this numerical scheme has been applied recently to treat the solidification of steel billets during continuous casting.[22]

A typical example of the experimental cooling curves for the five thermocouples during solidification of a Al 5 wt pct Cu alloy is shown in Figure 4(a). Experimental positions of liquidus isotherms as a function of time are shown in Figure 4(b) compared with the theoretical results furnished by the numerical solidification model, which used the corresponding value of the transient heat-transfer coefficient presented in Table II. A marked increase of the velocity of the tip interface near the end of the casting, given by the slope of this curve, can be observed. A good agreement has been observed between the experimental values and those numerically simulated for all the alloys and melt superheats experimentally examined. The numerical model, with the appropriate profile of transient heat-transfer coefficient, was then used to calculate the solidification thermal parameters associated with the CET transition: tip growth rate, thermal gradient in the liquid at the right of the tip interface, and cooling rate. These results are shown, respectively, in Figures 5 through 7.

Five examples of the directionally solidified macrostructures of Al 2, 5, 8, and 10 pct Cu alloys and Sn 10 pct Pb are shown in Figure 8. The lower parts of these ingots present a columnar structure and the upper parts an equiaxed one. The CET is observed to occur rapidly, essentially on a near horizontal plane, and further from the chill with increasing metal/mold heat-transfer coefficient and with increasing melt superheats. As observed by Wang and Beckermann,[3] the superheat effect is insignificant only for the low chill heat-transfer coefficient, being substantial for large cooling rates, and this is the case of the present experimental investigation.

Results of CET positions, v_L, G_L, and $\dot{T}$ at the transition, columnar (width), and equiaxed (diameter) grain sizes and secondary dendritic spacings on both sides of CET are listed in Table III for 15 tests on Al-Cu alloys, where d is the equiaxed grain size, l is the columnar grain width, and λ_2 represents the secondary dendrite arm spacings. It can be seen that the dendritic secondary spacings are essentially the same in the columnar and equiaxed structures for each experimental condition, exhibiting a slight increase at the equiaxed side of CET for the experiments performed with the Al 8 and 10 pct Cu alloys.

For one-dimensional heat flow conditions, the tip growth rate is coupled to the gradient, with high velocities at the chill face and low velocities in the upper part of the melt, up to the point where end effects[23,24] provoke an increase in growth rate, as shown in Figure 5. For the 100-mm-long ingots used in the present experiments, this was observed at about 70 to 80 mm from the metal/mold interface for the Al-Cu alloys. For the experimental situations examined in the present study, *i.e.*, one-dimensional heat flow under upward directional solidification conditions, with solute atoms heavier than those of the bulk liquid, convective fluid flow is minimized and only heat conduction in the liquid is significant. Under these conditions, a liquidus isotherm terminal speedup is expected if a melt superheat exists; otherwise, a continuous decrease in tip growth rate will occur in the system up to the end of solidification.[7,9,23,24] Lower temperature isotherms within the mushy zone, including the non-equilibrium solidus isotherm, will tend to accelerate after arrival of the liquidus isotherm at the end of the ingot, due to the progressive reduction in latent heat evolution.[23,24] In recent articles, Ares and Schvezov[11] and Gandin[12] have conducted experiments of upward solidification with lead-tin and aluminum-silicon alloys, respectively, and have reported a gradual increase in tip growth rate from bottom to top, in contradiction with the preceding discussion. As in both cases, the solute rejected into the liquid was lighter than the bulk, conditions for convective fluid flow were thus present, and this could explain, at least partially, the different behavior observed. Lateral heat losses, being

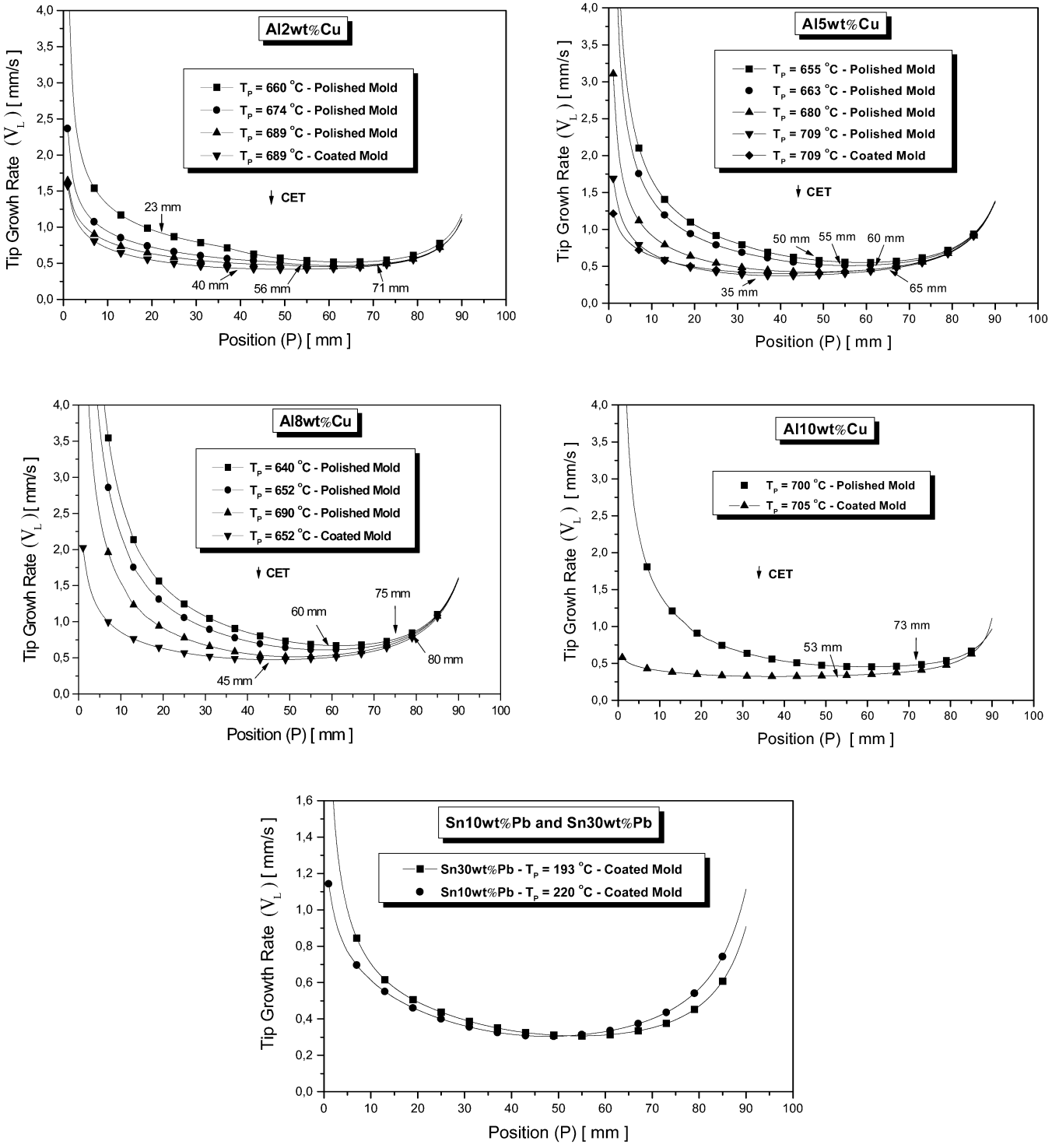

Fig. 5—Tip growth rate as function of position from metal/mold interface.

present, would also have a strong influence on the observed acceleration of tip growth rate.

As can be seen in Figure 5, there is no correlation between CET occurrence and the point where the tendency of the tip growth rate is reverted (tends to accelerate). As a matter of fact, CET has occurred for a range of tip growth rates. This makes clear that a CET criterion based only on tip growth rate is not consistent with the present experimental results. A similar conclusion can be drawn by examining the thermal gradient (G_L) evolution presented in Figure 6, or the G_L data corresponding to the structural transition listed in Table III. It can be seen that CET has occurred for G_L ranging from about 0.28 to 0.75 K/mm far from the 0.06 K/mm observed by Ziv and Weinberg[10] for Al 3 pct and 5 pct Cu alloys. These authors have also reported that no CET was observed when G_L was greater than 0.5 °C/mm. They have estimated the gradient ahead of the liquidus between thermocouples separated by 20 mm, and significant errors can be generated

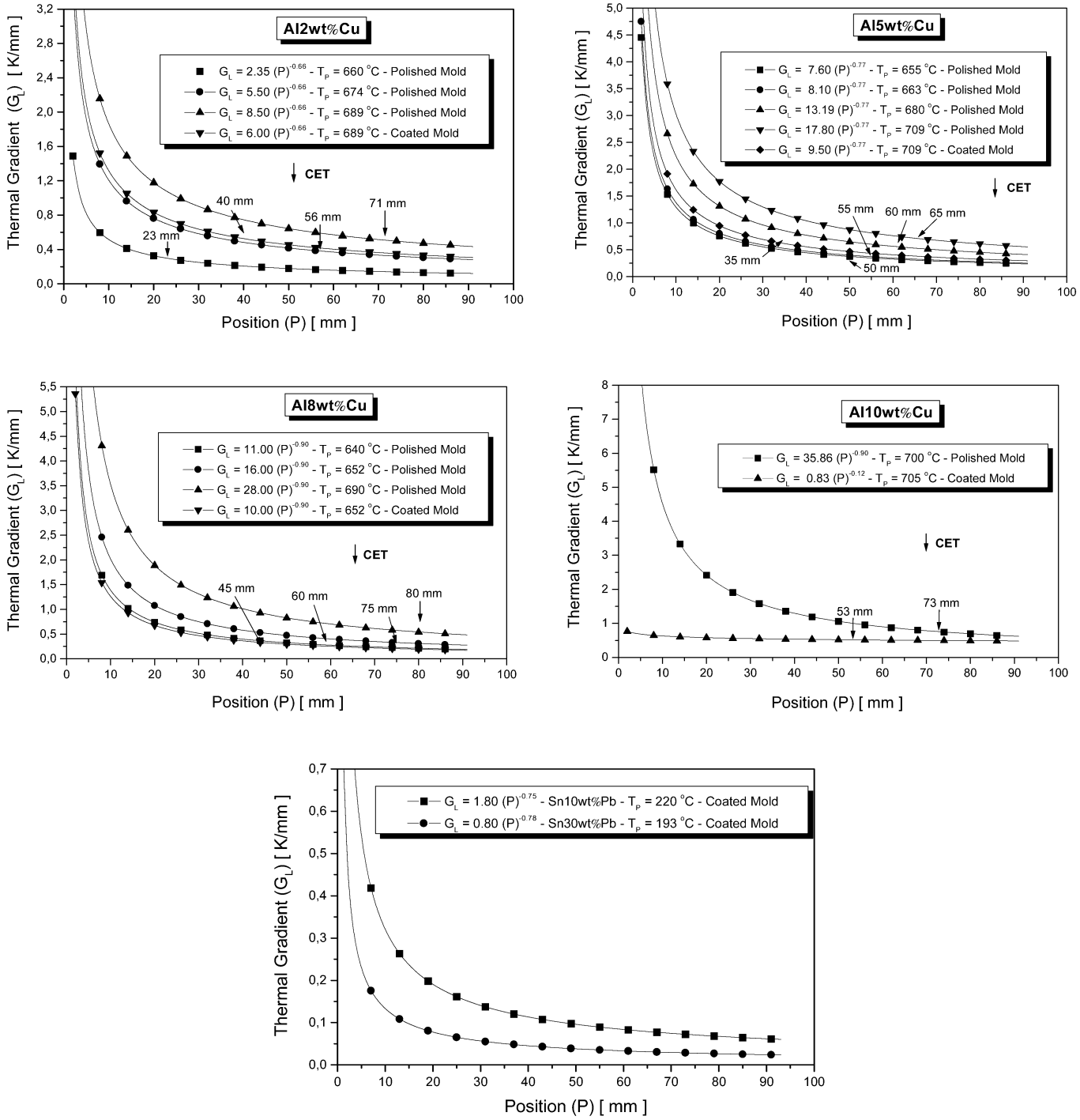

Fig. 6—Thermal gradient in the liquid ahead of liquidus isotherm as a function of position from metal/mold interface.

by such procedure, mainly when thermal gradients are considered. In the present investigation, as shown in Table III, from five experiments for the Al 5 pct Cu alloy, three presented $G_L > 0.5$ °C/mm at the CET position.

Suri *et al.*[7] developed a study of the columnar-to-equiaxed transition for Al 4.5 pct Cu alloy over a range of superheats and cooling rates and proposed a correlation to obtain the transition given by $G_L < 0.74\ v_L^{0.64}$. If this criterion is applied to the present experimental results concerning the Al 5 pct Cu alloy (Table III), we obtain the results given in Table IV.

It can be seen that only the two experiments with CET occurring for tip growth rates greater than 0.5 mm/s have supported the criterion.

By examining the curves presented in Figure 7, it seems that a more realistic criterion should encompass both the tip growth rate and the thermal gradient, through the tip cooling rate. It can be seen that, in all cases experimentally examined in the present study for Al-Cu alloys (15 different tests), a critical cooling rate of about 0.2 K/s can be related to the columnar-to-equiaxed transition. In the experiments performed with Sn-Pb alloys (10 and 30 wt pct), even when

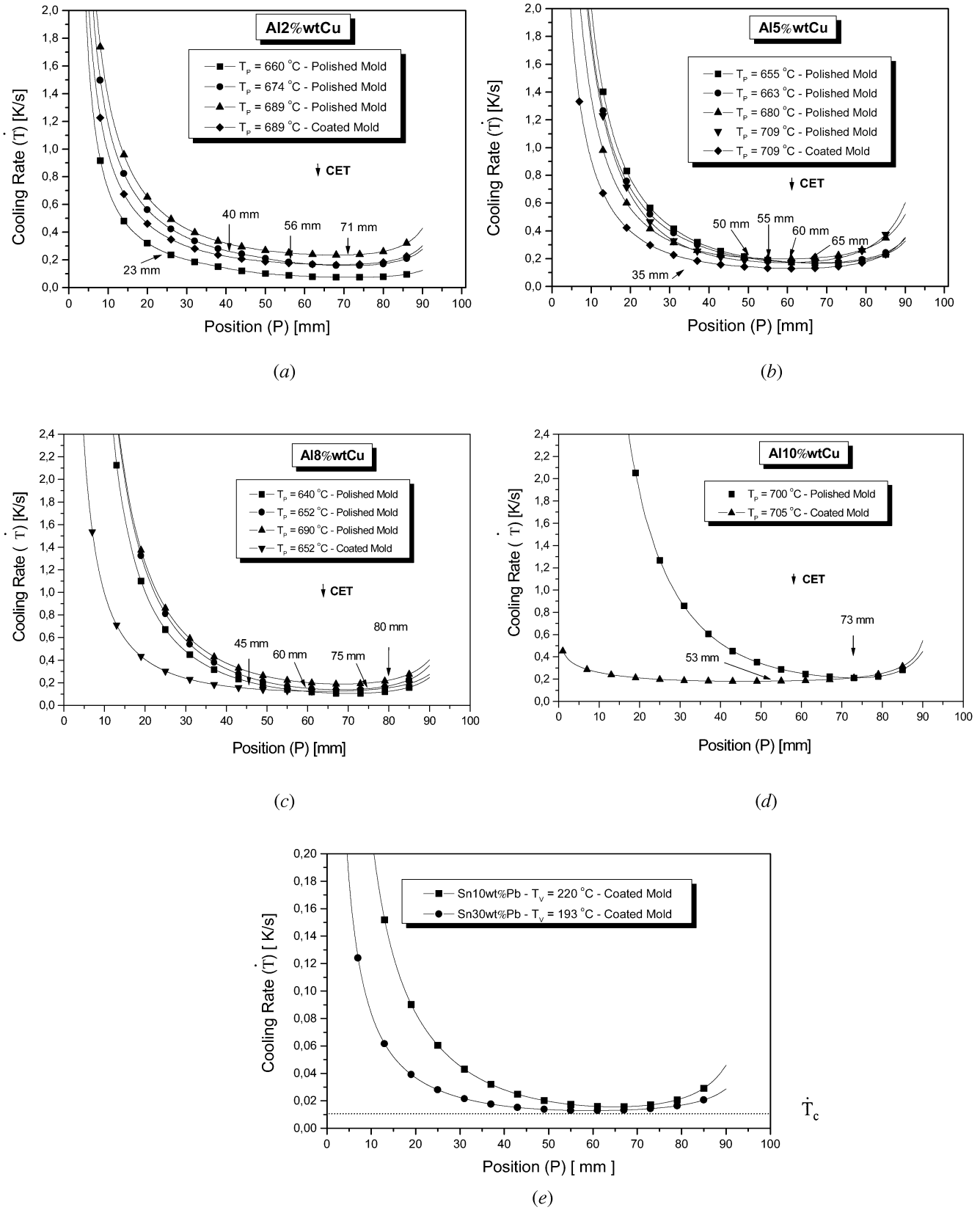

Fig. 7—Tip cooling rate as a function of position from metal/mold interface.

low heat-transfer coefficient profiles were imposed by a coated mold with an insulating layer of alumina, no CETs were observed and completely columnar structures were obtained. Mahapatra and Weinberg[9] have also used a numerical scheme to derive G_L and v_L to analyze the CET in Sn-Pb alloys directionally solidified. By calculating the

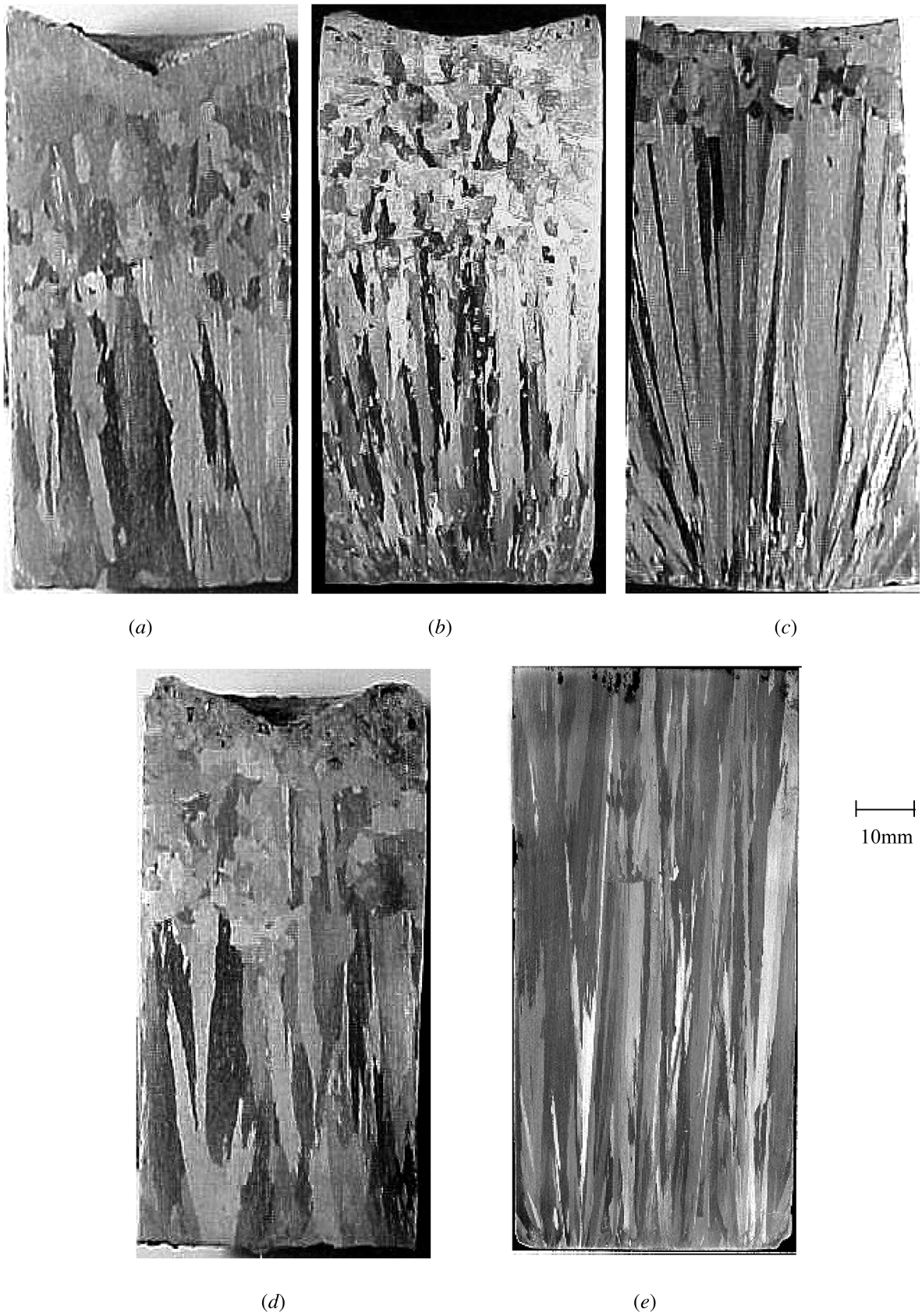

Fig. 8—Macrostructures: (*a*) Al 2 wt pct Cu, coated mold, and T_p = 689 °C; (*b*) Al 5 wt pct Cu, polished mold, and T_p = 680 °C; (*c*) Al 8 wt pct Cu, polished mold, and T_p = 690 °C; (*d*) Al 10 wt pct Cu, coated mold, and T_p = 705 °C; (*e*) Sn 10 wt pct Pb, coated mold, and T_p = 220 °C.

Table III. CET Positions, Thermal Parameters, Grain Sizes, and Secondary Dendritic Spacings

Alloy	T_p (°C)	CET (mm)	v_L (mm/s)	G_L (K/mm)	$\dot{T}$ (K/s)	l Columnar (mm)	d Equiaxed (mm)	λ_2 Columnar (μm)	λ_2 Equiaxed (μm)
Al 2 pct Cu	660 polished mold	23	0.879	0.297	0.261	0.55 ± 0.4	2.73 ± 0.7	*	*
	674 polished mold	56	0.483	0.386	0.186	0.92 ± 0.4	2.69 ± 0.7	*	*
	689 polished mold	71	0.493	0.510	0.251	1.63 ± 0.4	2.66 ± 0.7	*	*
	689 coated mold	40	0.463	0.526	0.243	3.96 ± 1.0	3.15 ± 0.9	81.03 ± 5.0	88.00 ± 5.0
Al 5 pct Cu	655 polished mold	50	0.575	0.374	0.215	1.83 ± 0.5	3.97 ± 0.8	62.81 ± 5.0	58.60 ± 5.0
	663 polished mold	55	0.517	0.370	0.191	1.85 ± 0.5	3.99 ± 0.8	61.90 ± 5.0	58.00 ± 5.0
	680 polished mold	60	0.358	0.564	0.201	1.82 ± 0.5	3.97 ± 0.8	60.11 ± 5.0	56.50 ± 5.0
	709 polished mold	65	0.312	0.715	0.223	1.85 ± 0.5	3.96 ± 0.8	61.20 ± 5.0	57.11 ± 5.0
	709 coated mold	35	0.337	0.615	0.207	4.35 ± 1.2	4.17 ± 1.0	74.03 ± 5.0	85.30 ± 5.0
Al 8 pct Cu	640 polished mold	60	0.613	0.276	0.170	2.58 ± 0.5	4.09 ± 1.0	41.03 ± 5.0	46.80 ± 5.0
	652 polished mold	75	0.466	0.328	0.153	2.26 ± 0.5	3.80 ± 1.0	39.92 ± 5.0	43.13 ± 5.0
	652 coated mold	45	0.507	0.325	0.165	4.07 ± 0.5	4.20 ± 1.0	73.85 ± 5.0	85.54 ± 5.0
	690 polished mold	80	0.419	0.542	0.227	2.19 ± 0.5	3.75 ± 1.0	48.90 ± 5.0	51.10 ± 5.0
Al 10 pct Cu	700 published mold	73	0.282	0.754	0.213	1.95 ± 0.5	3.73 ± 1.0	35.87 ± 5.0	37.40 ± 5.0
	705 coated mold	53	0.364	0.512	0.190	5.28 ± 1.0	3.90 ± 1.0	72.14 ± 5.0	82.10 ± 5.0

*Dendritic array not sufficiently defined to permit reliable spacing measurements.

Table IV. Experimental Values of V_L and G_L Compared with the Criterion Proposed by Suri *et al.*[7]

V_L (mm/s) CET Position	$G_L < 0.74\ v_L^{0.64}$	G_L (K/mm) CET Position
0.575	$G_L < 0.519$	0.374
0.517	$G_L < 0.485$	0.370
0.358	$G_L < 0.383$	0.564
0.312	$G_L < 0.351$	0.715
0.337	$G_L < 0.369$	0.615

critical cooling rate ($\dot{T}_c$) at the CET position from their results (13 experimental tests), a value of about 0.01 K/s can be found. This is indicated in Figure 7(e) compared to the cooling rate profiles determined in the present investigation. It can be seen that in both cases examined (Sn 10 and 30 pct Pb) this critical cooling rate is not attained and, consequently, no CET should occur.

An analytical heat-transfer model describing temperature distribution in the liquid, mushy zone, solid, and mold and the displacement of the solidus and liquidus isotherms during the unidirectional solidification of binary alloys can be used for determining expressions for temperature gradient (G_L) and growth rate at the dendrite tips (v_L) and, consequently, the tip cooling rate ($\dot{T}_L$).[25] The model is an extension of the one developed earlier by Garcia and Prates for pure metals cooled by fluids[26] and for pure metals solidifying against a massive uncooled substrate.[27] The model employs the mathematically expedient technique of replacing the interfacial resistance by equivalent layers of material, and the latent heat of fusion is taken into account by adjusting the specific heat over the solidification temperature range. The casting is treated as a one-dimensional moving boundary problem with boundaries at the solidus and liquidus isotherms. It is assumed that the Newtonian interface resistance is represented by a metal/mold heat-transfer coefficient h_i. The other thermophysical properties describing the system are treated as averages within the same phase. The model has been validated against experimental data describing the undirectional solidification of Al-Cu[25] and Zn-Al[28] alloys, and the agreement was found to be good. The temperature gradient and the growth rate at the dendrite tips are given, respectively, by

$$G_L = \left[\frac{m(T_p - T_{\text{Liq}})}{\sqrt{\pi}\cdot \alpha_{SL}\ \phi_2[1 - \text{erf}\ (m\phi_2)]\ \exp\ (m\phi_2)^2}\right] \cdot \frac{2\alpha_{SL}\ \phi_2^2}{\left[\frac{2K_s\ \phi_2\ (T_{\text{Sol}} - T_0)}{n\sqrt{\pi}\ (T_{\text{Liq}} - T_0)\ \exp\ (\phi_1^2)\ [M + \text{erf}\ (\phi_1)]h_i}\right] + S_L} \quad [10]$$

$$V_L = \frac{2\alpha_{SL}\ \phi_2^2}{\left[\frac{2K_S\ \phi_2\ (T_{\text{Sol}} - T_0)}{n\sqrt{\pi}\ (T_{\text{Liq}} - T_0)\ \exp\ (\phi_1^2)\ [M + \text{erf}\ (\phi_1)]h_i}\right] + S_L} \quad [11]$$

By multiplying Eqs. [10] and [11], the individual effects of alloy composition, melt superheat (ΔT_p), and metal/mold heat-transfer coefficient (h_i) on the CET can be seen inserted into an expression correlating tip cooling rate ($\dot{T}_L$) and solidification parameters, given by

$$\dot{T}_L = \left[\frac{m\Delta T_p}{\sqrt{\pi}\cdot \alpha_{SL}\ \phi_2\ [1 - \text{erf}\ (m\ \phi_2)]\ \exp\ (m\ \phi_2)^2}\right] \left[\frac{2\alpha_{SL}\ \phi_2^2}{\frac{2K_s\ \phi_2\ (T_{\text{Sol}} - T_0)}{n\ \sqrt{\pi}\ (T_{\text{Liq}} - T_0)\ \exp\ (\phi_1^2)\ [M + \text{erf}\ (\phi_1)]h_i} + S_L}\right]^2 \quad [12]$$

where m is the square root of ratio of thermal diffusivities of mushy zone and liquid, α_{SL} is the mushy zone thermal diffusivity, ϕ_1 and ϕ_2 are solidification constants associated with the displacement of solidus and liquidus isotherms, K_S is the solid thermal conductivity, T_{Sol} is the nonequilibrium solidus temperature, T_0 is the environment temperature, T_{Liq} is the liquidus temperature, n is the square root of the ratio

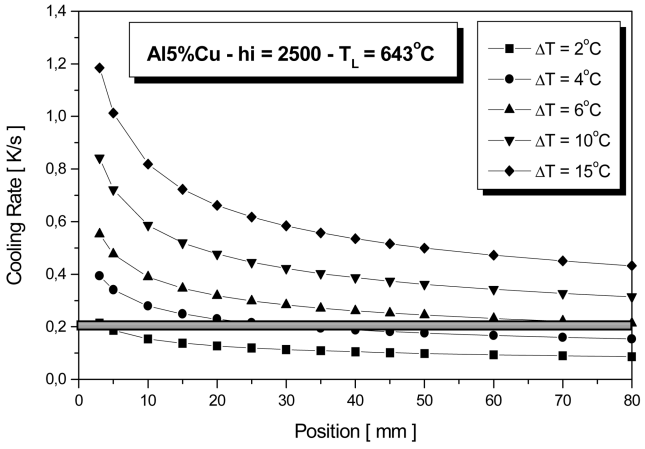

(*a*)

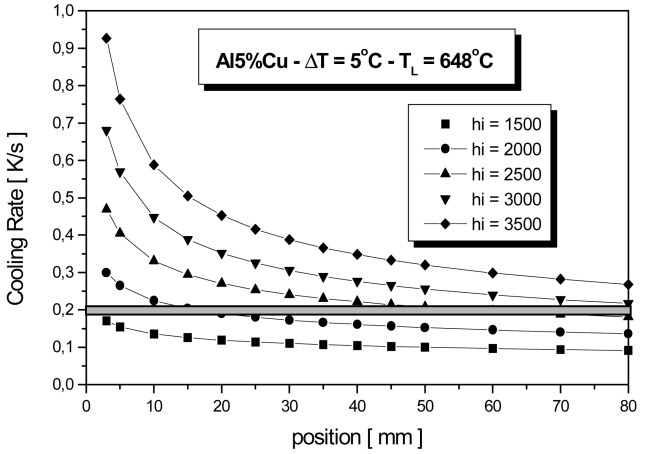

(*b*)

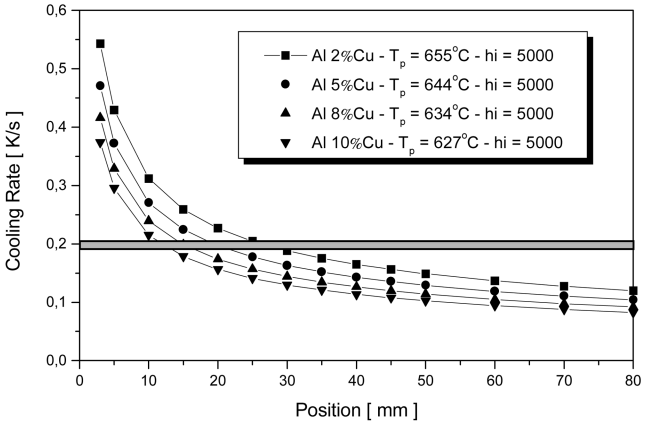

(*c*)

Fig. 9—Simulations with Eq. [12]: (*a*) Al 5 wt pct Cu, $h_i = 2500$ W/m^{2}K, and different melt superheats; (*b*) Al 5 wt pct Cu, melt superheat of 5 K, and different values of h_i (W/m^{2}K); (*c*) $h_i = 5000$ W/m^{2}K, 1 K superheat, and different solute contents. Critical cooling rate $\dot{T}_c = 0.2$ K/s.

of thermal diffusivities of solid and mushy zone, M is the ratio of heat diffusivities of solid and mold material, and S_L is the position of liquidus isotherm from metal/mold interface. The CET is expected to occur when $\dot{T}_L$ decreases to a critical value that seems to depend only on the alloy system. Figure 9 illustrates the results of calculations performed with Eq. [12] for a Al 5 wt pct Cu alloy under different conditions of melt superheat (A), metal/mold heat-transfer coefficients (B), and Al-Cu alloys of different solute contents (C_0), compared with the critical cooling rate.

IV. CONCLUSIONS

Experiments were conducted to analyze the columnar-to-equiaxed transition during the upward unsteady-state directional solidification of Al-Cu and Sn-Pb alloys. The following conclusions can be drawn.

1. The CET was observed to occur essentially on a near horizontal plane whose distance from the chill increased with increasing heat-transfer coefficient and with increasing melt superheat.
2. For the one-dimensional heat flow conditions experimentally examined, the tip growth rate is coupled to the thermal gradient, with high velocities at the chill face and low velocities in the upper part of the casting, up to the point where end effects provoke an increase in growth rate. This liquidus isotherm speedup induces an increase in tip cooling rate.
3. The CET has occurred, for Al-Cu alloys, for tip growth rates ranging from 0.28 to 0.88 mm/s and without any correlation with the growth rate reversion point, making it clear that a CET criterion based only on tip growth rate is not consistent with the present experimental results.
4. The CET has occurred, for Al-Cu alloys, for values of temperature gradient in the melt ahead of the liquidus isotherm ranging from 0.28 to 0.75 K/mm. Comparison with other experimental results from the literature do not give support to a CET criterion based only on thermal gradient.
5. It seems that a more realistic CET criterion should encompass both the tip growth rate and the thermal gradient, through the tip cooling rate. The columnar growth is observed to prevail throughout the casting for cooling rates higher than a critical value, which depends only on the alloy system. In the present investigation, the critical cooling rate was observed to be about 0.2 K/s for Al-Cu alloys and 0.01 K/s for Sn-Pb alloys.

ACKNOWLEDGMENTS

The authors acknowledge financial support provided by FAEP-UNICAMP, FAPESP (The Scientific Research Foundation of the State of São Paulo, Brazil), and CNPq (The Brazilian Research Council).

REFERENCES

1. S.C. Flood and J.D. Hunt: in *Metals Handbook*, ASM INTERNATIONAL, Materials Park, OH, 1988, vol. 15, pp. 130-36.
2. M.H. Burden and J.D. Hunt: *Metall. Trans. A*, 1975, vol. 6A, pp. 240-41.

3. C.Y. Wang and C. Beckermann: *Metall. Mater. Trans. A*, 1994, vol. 25A, pp. 1081-93.
4. L.A. Tarshis, J.L. Walker, and J.W. Rutter: *Metall. Trans.*, 1971, vol. 2, pp. 2589-97.
5. R.D. Doherty, P.D. Cooper, M.H. Bradbury, and F.J. Honey: *Metall. Mater. Trans. A*, 1977, vol. 8A, pp. 397-402.
6. S. Witzke and J.P. Riquet: *Acta Metall.*, 1982, vol. 30, pp. 1717-22.
7. V.K. Suri, N. El-Kaddah, and J.T. Berry: *AFS Trans.*, 1991, vol. 99, pp. 187-91.
8. H. Fredriksson and A. Olsson: *Mater. Sci. Technol.*, 1986, vol. 2, pp. 508-16.
9. R.B. Mahapatra and F. Weinberg: *Metall. Trans. B*, 1987, vol. 18B, pp. 425-32.
10. I. Ziv and F. Weinberg: *Metall. Trans. B*, 1989, vol. 20B, pp. 731-34.
11. A.E. Ares and C.E. Schvezov: *Metall. Mater. Trans. A*, 2000, vol. 31A, pp. 1611-25.
12. Ch-A. Gandin: *Acta Mater.*, 2000, vol. 48, pp. 2483-501.
13. J.D. Hunt: *Mater. Sci. Eng.*, 1984, vol. 65, pp. 75-83.
14. S.C. Flood and J.D. Hunt: *Appl. Sci. Res.*, 1987, vol. 44, pp. 27-42.
15. S.C. Flood and J.D. Hunt: *J. Cryst. Growth*, 1987, vol. 82, pp. 543-51.
16. S.C. Flood and J.D. Hunt: *J. Cryst. Growth*, 1987, vol. 82, pp. 552-60.
17. J.A. Spim and A. Garcia: *Mater. Sci. Eng. A*, 2000, vol. 277, pp. 198-05.
18. J.A. Spim and A. Garcia: *Num. Heat Transfer B*, 2000, vol. 38, pp. 75-92.
19. C.A. Santos, J.M.V. Quaresma, and A. Garcia: *J. Alloys Compounds*, 2001, vol. 319, pp. 174-86.
20. F.P. Incropera and D.P. Dewit: *Fundamentals of Heat and Mass Transfer.*, Wiley, New York, NY, 1990.
21. V.L. Voller and C.R. Swaminathan: *Numer. Heat Transfer B*, 1991, vol. 19, pp. 175-89.
22. N. Cheung and A. Garcia: *Eng. Appl. Artificial Intelligence*, 2001, vol. 14, pp. 229-38.
23. T.W. Clyne: *Metall. Trans. B*, 1982, vol. 13B, pp. 471-78.
24. D. Bouchard and J.S. Kirkaldy: *Metall. Mater. Trans. B*, 1996, vol. 27B, pp. 101-13.
25. J.M.V. Quaresma, C.A. Santos, and A. Garcia: *Metall. Mater. Trans. A*, 2000, vol. 31A, pp. 3167-78.
26. A. Garcia and M. Prates: *Metall. Trans. B*, 1978, vol. 9B, pp. 449-57.
27. A. Garcia, T.W. Clyne, and M. Prates: *Metall. Trans. B*, 1979, vol. 10B, pp. 85-92.
28. W.R. Osorio and A. Garcia: *Mater. Sci. Eng. A*, 2002, vol. 325, pp. 104-12.